CrossMark

Orientation of β-cyclodextrin onto metal oxides and its paradoxical role in photocatalytic decoloration of 4-nitrophenol

Rajalakshmi Subramanian[1] · Velusamy Ponnusamy[2]

Abstract Increasing interest has been devoted to use the metal oxides (MOs = TiO_2 and ZnO)/β-cyclodextrin (β-CD) as a photocatalysts for potential application in photo catalysis. By taking TiO_2 and ZnO as a metal oxides, we conceptually demonstrate the enhancement of catalytic activity of MOs by β-CD for the photocatalytic decoloration of 4-NP. The present study reveals the ability of β-CD as a low cost co-catalyst for the enhancement of photocatalytic activity. The promising characteristics of MOs/β-CD may have the potential use in various indoor applications. Powder X-ray diffraction analyses results showed that the slight increase in the crystal size of MOs/β-CD leads to a small decrease in the surface area. It is hoped that this work offers a valuable source of reference on application of MO/β-CD as a photo catalysts in the environmental cleanup.

1 Introduction

With the acceleration of economic development and human activities, the destruction of the integrity of water sources has become more serious, requiring intervention [1]. Phenolic hydrocarbons including nitrophenols are widely used in pharmaceutical, petrochemical and other chemical manufacturing processes. Because of their harmful effects, wastewater containing phenolic compounds must be treated before being discharged into receiving water bodies. The methods for treating wastewater containing phenolic compounds can be classified into biological, physical and chemical methods. The reaction rates of the biological methods are usually slow; thus huge reactor volumes or spaces are usually required. The physical methods only transform the pollutants into other forms; thus new waste disposal problems are generated. The reaction rates of the chemical methods are relatively high and total mineralization is possible if the reaction conditions and reactor are adequately designed. Among the many chemical methods, the advanced oxidation process (AOP) using the hydroxyl radical (˙OH) has been recognized as a promising technology to treat wastewater containing refractory organic compounds [2, 3].

In recent years, semiconductors based photocatalysis has become the focus of numerous investigations owing to its potential applications in thoroughly decomposing undesirable organic contaminants in wastewater and air. Among various metal oxide semiconductor materials, TiO_2 and ZnO have been most frequently employed as a promising photocatalysts because of their various merits, such as optical–electronic properties, chemical stability, low cost and non-toxicity [4]. However, the practical applications of TiO_2 and ZnO have been suppressed due to the following two drawbacks: (1) low quantum yield that arises from the rapid recombination of photo-induced electrons and holes; (2) poor solar efficiency that is determined their band gap [5, 6].

Cyclodextrins (CDs), a class of cyclic oligosaccharides with 6–8 D-glucose units linked by α-1,4-glucose bonds served as the starting materials to construct the supramolecular architectures. The truncated cone-shaped hydrophobic cavities of CDs have a remarkable ability to

✉ Velusamy Ponnusamy
velusamyanjac@rediffmail.com

Rajalakshmi Subramanian
chemrajimani@gmail.com

[1] Department of Chemistry, Erode Arts and Science College, Erode, Tamilnadu 638 009, India

[2] Centre for Research and Post-graduate Studies in Chemistry, Ayya Nadar Janaki Ammal College, Sivakasi, Tamilnadu 626 124, India

include various guest molecules either in solution state or in the solid state to form the functional host–guest inclusion complexes which can be subsequently used as the building blocks of supramolecular aggregates. Among the various families of organic compounds used as guest molecules, the chromophoric guests, such as nitrobenzenes are of particular importance because they can exhibit appreciable spectral changes upon complexation by inclusion with CDs in solution [7].

To the best of our knowledge, no previous work regarding the application of β-CD on the photocatalytic decoloration of 4-nitrophenol (4-NP) has been reported. Although β-CD possesses many unique properties, its applications as catalyst are still scarce. Herein, we report the photocatalytic decoloration of 4-NP with metal oxides (MOs)/β-CD nanocomposites. The nanocomposites are also characterized by UV-DRS, FE-SEM and PXRD analyses. The formation of inclusion complex between 4-NP and β-CD is also studied by UV–visible, FT-IR and ^{1}H NMR spectral studies. This paper contributes to study the photocatalytic behaviour of the MOs/β-CD for environmental remediation.

2 Experimental

2.1 Materials

4-NP was purchased from Loba Chemie (P) Ltd. TiO$_2$ and ZnO were obtained from Merck. β-CD was purchased from Hi media Chemicals (P) Ltd. The physical properties of 4-NP and β-CD are given in Table 1. All other reagents were used as received without further purification.

2.2 Preparation of 4-NP/β-CD complex

4-NP/β-CD complex was prepared by mixing an equimolar ratio of 4-NP and β-CD in an aqueous solution followed by stirring for 24 h and evaporated to dryness. The resultant solid is a yellow flaked product. The precipitated inclusion complex was washed with diethyl ether to remove uncomplexed 4-NP and dried in an air oven at 60 °C for 3 h. The physical mixture of 4-NP and β-CD was prepared by mixing an equimolar amount of 4-NP and β-CD and crushed them thoroughly in an agate mortar resultant mixture is a yellowish white powder.

2.3 Preparation of MOs/β-CD

MOs such as TiO$_2$ and ZnO were added into 0.01 mol/L β-CD solution and stirred for 20 min. The suspended solution was centrifuged; the solids were separated and washed

three times with water. The solid was dried and used for analyses.

2.4 Photocatalytic activity

Experiments for the characterization of the photocatalytic decoloration process were generally carried out with a 1000 mg/L 4-NP solution. The other conditions such as total volume, required amount of catalysts and solution pH were kept throughout this work as constant if special requirement was not involved. The catalyst was first mixed well into 4-NP solution and the equilibrated suspension was obtained by adequate agitation and then placed in dark container for 30 min at least. The suspension was irradiated by UV light and sampled at specific intervals to monitor the change of leftover concentration of 4-NP. The sampled suspension was centrifuged at 4000 rpm for 20 min to precipitate the MOs powder and the centrifugate was analyzed by visible spectrophotometer. COD analyses were done by open reflux method [8].

2.5 Analysis

X-ray diffraction patterns of powder samples were recorded with a high resolution powder X-ray diffractometer model RICH SIERT and Co with Cu K$_\alpha$ radiation as the X-ray source ($\lambda = 1.5406 \times 10^{-10}$ m). FE-SEM images were obtained from Carl ZEISS (ΣIGMA Series, Germany) microscope taken at an accelerated voltage of 2 kV. UV–visible diffuse reflectance spectra were recorded in Shimadzu 2550 UV–visible spectrophotometer with BaSO$_4$ as the background between 200 and 800 nm. NMR spectra were recorded at 400 MHz Bruker NMR spectrometer (in DMSO–d$_6$). UV–visible spectra were recorder using UV–visible spectrophotometer (Shimadzu UV-1700) with the scan range from 200 to 800 nm. FT-IR spectra were recorded using FT-IR spectrometer (Shimadzu model 8400S) in the region 4000–500 cm^{-1} using KBr pellets. Absorbance of the 4-NP was determined with visible spectrophotometer (ELICO-207). The pH of 4-NP solution was measured by using digital pen pH meter (HANNA Instrument, Portugal).
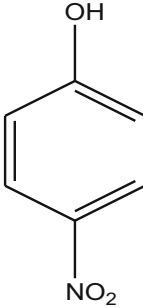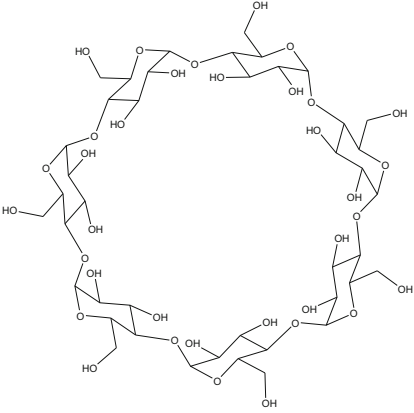
3 Results and discussion

3.1 Characterization of photocatalysts

3.1.1 Morphology of photocatalysts

FE-SEM observations can reveal that the catalysts consisted of aggregates of particles. Figure 1a–e shows the representative micrographs obtained for the bare β-CD,

Table 1 Physical properties of 4-NP and β-CD

Name	4-NP	β-CD
Molecular formula	$C_6H_5NO_3$	$C_{42}H_{70}O_{35}$
Molecular weight	139.11	1135.0
Appearance	Yellow powder	White powder
pH	3.3	–
λ_{max}	340 nm	–
Structure		

TiO_2, ZnO, TiO_2/β-CD and ZnO/β-CD nanocomposites. It can be observed that the microsphere possesses a similar surface condition and presents numerous uniformly spherical and hexagonal structures of TiO_2 and ZnO, indicating that the MOs microspheres were basically no change in bare and in TiO_2/β-CD and ZnO/β-CD nanocomposites. It is also observed that the surface of MOs nanocomposites (TiO_2/β-CD and ZnO/β-CD) is very loosely backed in nature. This kind of surface can provide a better adsorption environment and more active sites for the photocatalytic decoloration reactions [9, 10].

3.1.2 Phase structure

The powder X-ray powder diffraction patterns of β-CD, TiO_2, TiO_2/β-CD, ZnO and ZnO/β-CD nanocomposites are presented in Fig. 2a–e. For TiO_2 the peaks corresponding the anatase TiO_2 phase appeared at $2\theta = 25.3°$, 37.8°, 48.0° and 54.4° (JCPDS card 21-1272). Moreover, no significant rutile phase was observed in both TiO_2 and TiO_2/β-CD because of the absence of the (110) rutile reflection at $2\theta \sim 27.4°$. For ZnO all the diffraction peaks could be indexed to hexagonal wurtzite structure of ZnO (JCPD no. 36-1451). It is obvious that the (100), (002) and (101) planes possess the highest intensities indicative of anisotropic growth of the ZnO. The PXRD pattern of the ZnO/β-CD shows that the diffraction peaks are also in good agreement with those of hexagonal ZnO and are almost identical to that of the bare ZnO indicating that in ZnO/β-CD no new phase was formed. It is interesting to note that compared to that of the bare ZnO the diffraction

peaks of the ZnO/β-CD became sharper and narrower revealing increased size and improved crystallinity [11, 12].

The average crystal sizes of the nanocomposites have been deduced from the half-width of the full maximum (HWFM) of the most intense peaks of the TiO_2, TiO_2/β-CD, ZnO and ZnO/β-CD using the Scherrer equation, $D = 0.9\lambda/\beta \cos\theta$, where D is the mean crystallite size, λ is the X-ray wavelength, θ is the Bragg angle and β is the corrected line broadening of the sample [13]. The specific surface area (S) of the nanocrystal can be obtained using the relationship, $S = 6/\rho D$, where S is the specific surface area, D is the average particle size and ρ is the material density. The results are presented in Table 2. The mean crystallite size of MOs/β-CD is slightly larger than its corresponding MO. The slight increase in the crystal size of MOs/β-CD leads to a small decrease in the surface area [14, 15].

3.1.3 Optical properties

Figure 3 (inset) shows the UV–DRS absorption spectra of all the MOs/β-CD nanocomposites along with the bare MOs. β-CD added with metal oxides significantly affected the light absorption property of the photocatalysts. It is noticeable that the light absorption of MOs/β-CD nanocomposites in the visible light range is higher than that of bare MOs. Furthermore, a slight red shift of the optical absorption edge is observed for MOs/β-CD compared to bare MOs. The observed red shift indicates the narrower band gap originated due to the charge transfer between
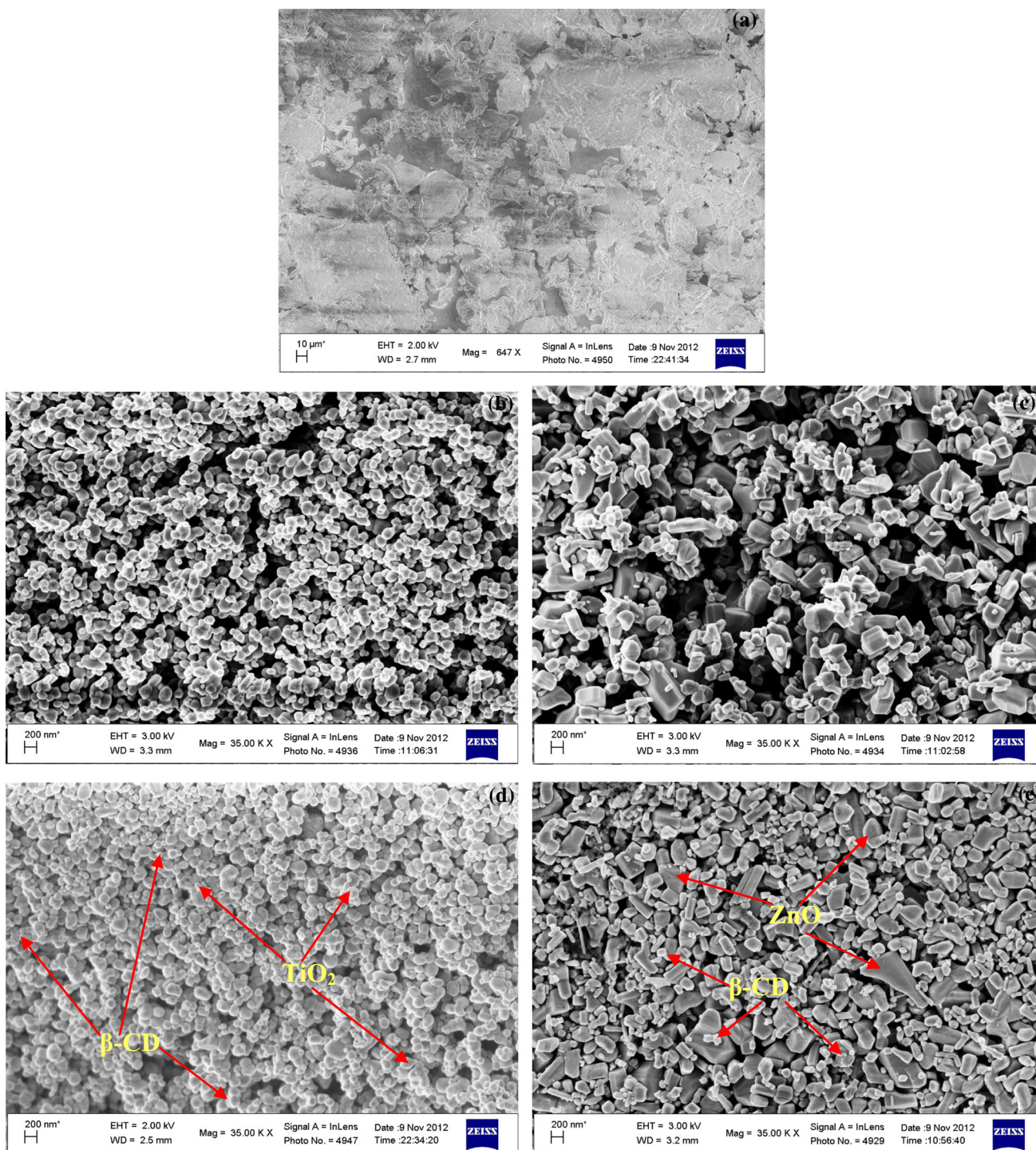
Fig. 1 FE-SEM images of **a** β-CD, **b** TiO_2, **c** ZnO, **d** TiO_2/β-CD, **e** ZnO/β-CD

valence or conduction band of MOs. Hence, the absorption property deduced that the MOs/β-CD could be promising catalysts for photocatalysis. The reflectance data reported as $(\alpha h\nu)^2(eV)^2$ values have been obtained by the application of the Kubelka–Munk algorithm. The band gaps of the catalysts have been deduced from the Tauc plot. Figure 3 indicates the plot of $(\alpha h\nu)^2(eV)^2$ versus Band gap energy.

The extrapolation of the rising segment of $(\alpha h\nu)^2(eV)^2$ to the abscissa at zero F(R) provides the band gap energy as 3.35 eV (TiO_2), 3.27 eV (ZnO), 3.31 eV (TiO_2/β-CD) and 3.23 eV (ZnO/β-CD). The results showed that the band gap energy of MOs/β-CD nanocomposites is lower than the corresponding MOs. Therefore, MOs/β-CD nanocomposites can be excited to produce more electron–hole pairs
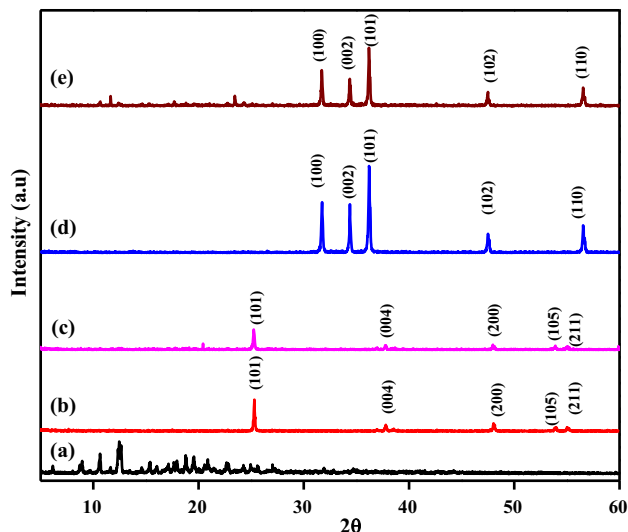
Fig. 2 Powder XRD Pattern for *a* β-CD, *b* TiO₂, *c* TiO₂/β-CD, *d* ZnO, *e* ZnO/β-CD

Table 2 Average particle size and specific surface area of nanocomposites

Nanocomposites	Average particle size (D; nm)	Specific surface area (S; m²/g)
TiO₂	2.08	64.6
ZnO	1.65	93.2
TiO₂/β-CD	2.51	60.6
ZnO/β-CD	1.69	91.6
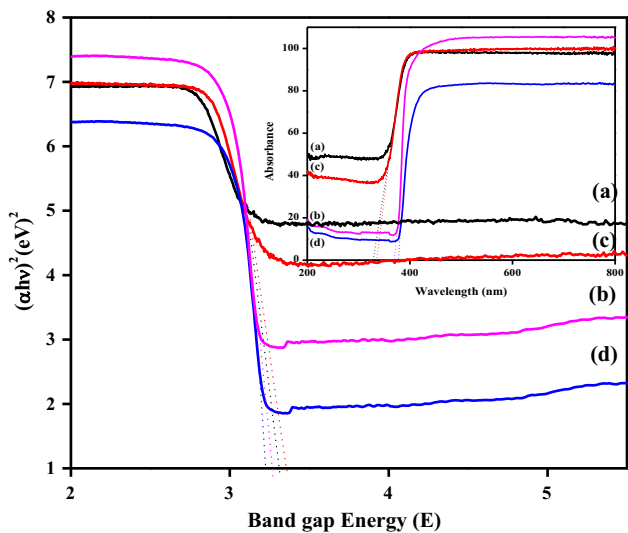
Fig. 3 Tauc plot and (*inset*) absorption spectra of *a* TiO₂, *b* ZnO, *c* TiO₂/β-CD, *d* ZnO/β-CD

compared to that of bare MOs under same light illumination which could result in higher photocatalytic activity [15].

From the position of the spectral absorption edge of each catalysts (nm), the average particles size can be determined using Henglein's empirical relation between particles size and absorption onset according to the following equation:

$$2R = 0.1/(0.138 - 0.0002345\,\lambda)\text{nm} \qquad (1)$$

where 2R is the diameter of the particles. An average diameter of 2.04, 1.62, 2.46 and 1.64 nm was estimated for TiO₂, ZnO, TiO₂/β-CD and ZnO/β-CD respectively which is slightly smaller than that calculated by XRD (Table 2) [16].

3.2 Evidence for the formation of 4-NP/β-CD complex

3.2.1 Dissociation constant measurement

The dissociation constant is established from Benezi–Hildebrand equation (Figs. 4, 5) [17]. The K_D value is 1.16×10^{-3} M. This shows that there is a strong inclusion complex was formed between 4-NP and β-CD.
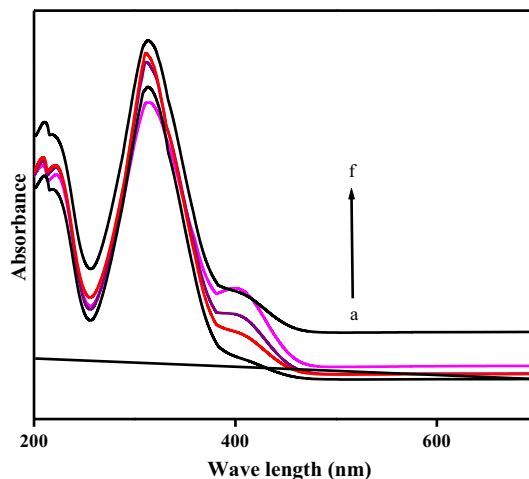

Fig. 4 UV–visible spectra for complexation of 4-NP/β–CD complex. *a* β-CD, *b* 4-NP, *c* 1:1 4-NP/β-CD, *d* 1:2 4-NP/β-CD, *e* 1:3 4-NP/β-CD
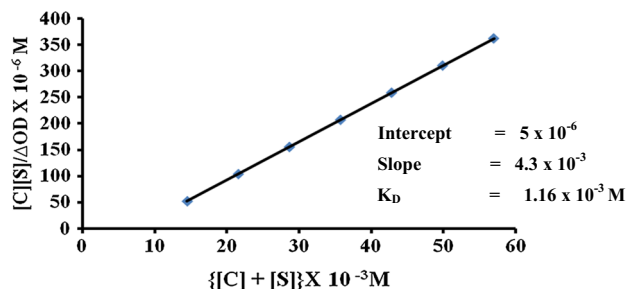

Fig. 5 Plot of [C] [S]/Δ OD versus {[C] + [S]} for 4-NP/β-CD complex

3.2.2 FT–IR spectra

FT-IR spectra of β-CD, 4-NP, 1:1 physical mixture of 4-NP and β-CD and 1:1 complex mixture of 4-NP and β-CD are presented in Fig. 6, the aromatic C–H stretching observed at 3323.12 cm^{-1} is shifted with intensity to 3359.77 cm^{-1} in the complexation mixture. Similarly, –C=C–, –N=O– and aromatic –NO$_2$ stretching corresponding to frequencies such as 1589.23, 1492.80 and 819.69 cm^{-1} is shifted to 1595.02, 1500.52 and 846.69 cm^{-1} respectively. This confirms that the phenyl ring present in the 4-NP protrude into the cavity of β-CD to form inclusion complex between 4-NP and β-CD.

3.2.3 ^{1}H NMR analysis

^{1}H NMR provides further information about the formation of 4-NP/β-CD complex. The chemical shifts in ppm given for β-CD protons are shifted in 4-NP/β-CD complex. The values of chemical shifts, δ for different protons in β-CD and 4-NP/β-CD inclusion complex are listed in Table 3 and given in Fig. 7. It can be seen from the ^{1}H NMR that in inclusion complex, an upfield shift was occurred for H_1, H_3 and H_5 protons and downfield shift for H_2 and H_4 protons. H_6 proton does not undergo any changes. The change of chemical shift ($\Delta\delta$) of H_3 and H_5 proves that the 4-NP molecules strongly encapsulated into the hydrophobic cavity of β-CD. Similarly, the chemical shifts of H_c and H_e of 4-NP are also shifted to downfield and H_b and H_f shifted to upfield significantly because of the interaction between 4-NP and β-CD. Such changes in chemical shifts values are felt as a consequence of anisotropic effects of the aromatic ring residing inside the cavity and considered to be
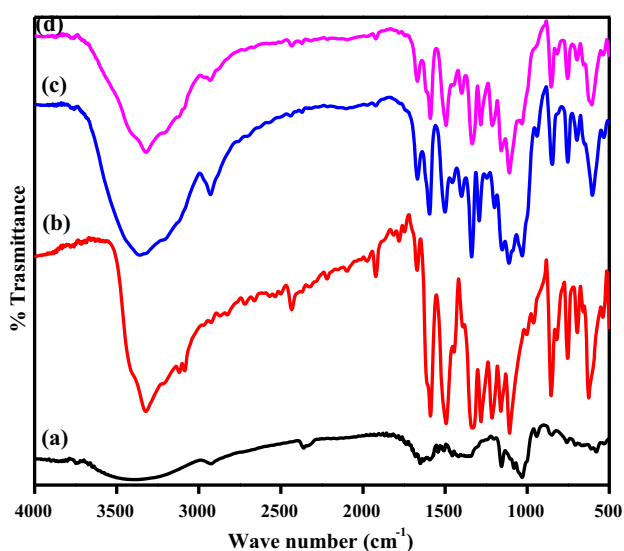

Fig. 6 FT-IR spectra of *a* β-CD, *b* 4-NP, *c* 1:1 Physical mixture of 4-NP/β-CD, *d* 1:1 complex of 4-NP/β-CD

evidence for inclusion complex formation in aqueous β-CD solution [18–20].

3.3 Photocatalytic decoloration experiments

3.3.1 Effect of initial concentration of 4-NP

The photocatalytic decoloration of 4-NP under UV light irradiation is studied in the concentration ranges from 0.3 to 1.8×10^{-4} M (TiO$_2$); $1.4–7.1 \times 10^{-4}$ M (ZnO); $1.7–8.9 \times 10^{-4}$ M (TiO$_2$/β-CD); $17.9–89.8 \times 10^{-4}$ M (ZnO/β-CD) at constant amount of catalysts 2 g/L for TiO$_2$ and ZnO and 0.2 g/L for TiO$_2$/β-CD and ZnO/β-CD, pH 3.3. As seen in the Fig. 8, percentage of decoloration is inversely affected by the concentration of 4-NP. This negative effect can be explained as follows–as the concentration of 4-NP is increased, the equilibrium adsorption of 4-NP molecules on the catalyst surface active sites increases; hence competitive adsorption of O$_2$ on the same sites decreases, meaning a lower formation rate of O$_2^{\cdot}$, H$_2$O$_2$ an ˙OH radical, which are principal oxidant necessary for a high percentage of decoloration. On the other hand, considering the Beer–Lambert law as the initial concentration of 4-NP increases the path length of photons entering the solution decreases, resulting in lower photon adsorption on catalyst particles and consequently a lower percentage of decoloration of 4-NP [21–23].

3.3.2 Effect of irradiation time

Irradiation time plays an important role in photocatalytic decoloration process. It has been observed from the Fig. 9 that the percentage of decoloration increases with increase in irradiation time from 65.2 to 90.0% for MO system and from 83.0 to 99.6% for MO/β-CD system. As time proceeds, this concentration gradient decreases due to accumulation of organic molecules on vacant sites and thus saturation stage was almost perceived and hence percentage of decoloration increases [23].

3.3.3 Photocatalytic decoloration kinetics of 4-NP

When photocatalytic decoloration of 4-NP was performed in varying initial concentration, the results demonstrated that conversion were less in the solution of higher initial concentration of 4-NP when compared to the conversions in the lower concentration solutions. This can be ascribed to the decrease in the number of active sites on the catalyst surface due to the covering of the surface with 4-NP molecules which is directly proportional with the initial concentration of 4-NP. The relationship between the initial decoloration rate (r) and the initial concentration of the organic substrate for heterogeneous photocatalytic

Table 3 ^{1}H NMR chemical shifts of 4NP and β-CD protons in 4-NP/β-CD complex

β-CD							4-NP	
	H_1	H_2	H_3	H_4	H_5	H_6	H_b and H_f	H_c and H_e
4-NP and β-CD	5.03	4.00	3.73	3.02	3.73	3.54	6.99	8.02
4-NP/β-CD	4.83	4.46	3.62	3.32	3.62	3.54	6.93	8.10
Δδ	0.20	−0.46	0.11	−0.30	0.11	0.00	0.06	−0.08

Chemical shifts values are expressed in ppm
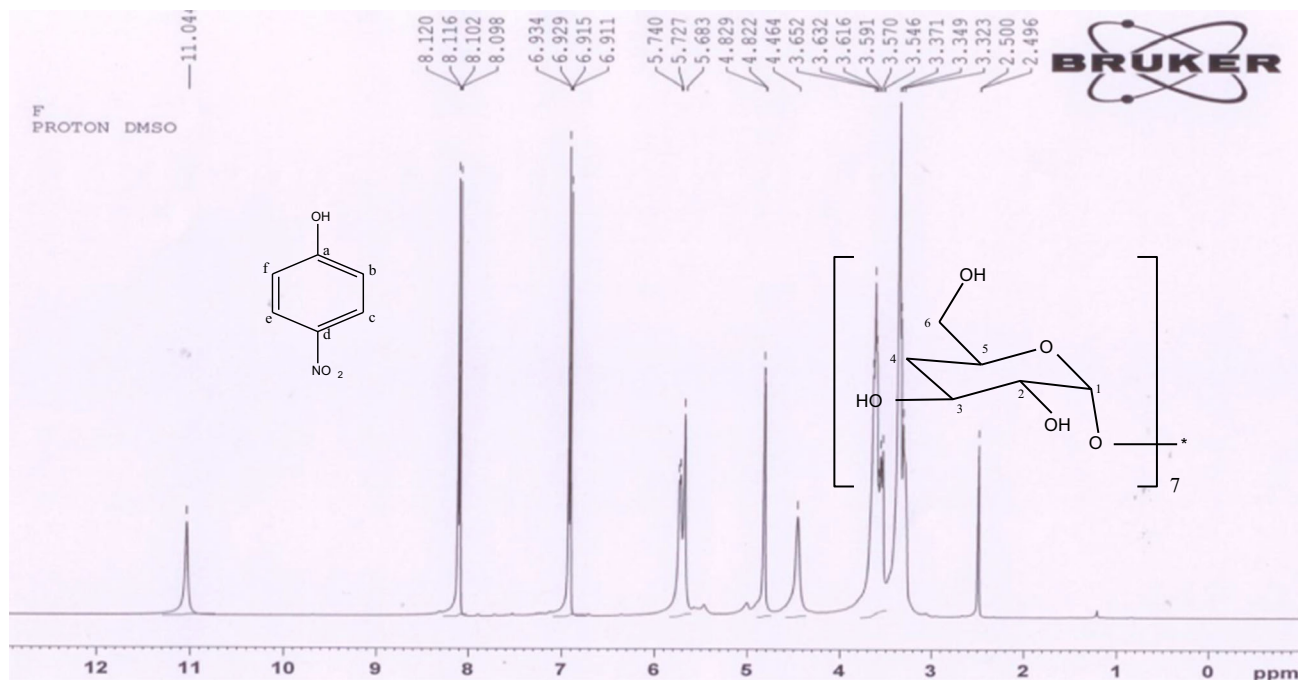
Fig. 7 ^{1}H NMR spectra of 4-NP/β-CD inclusion complex
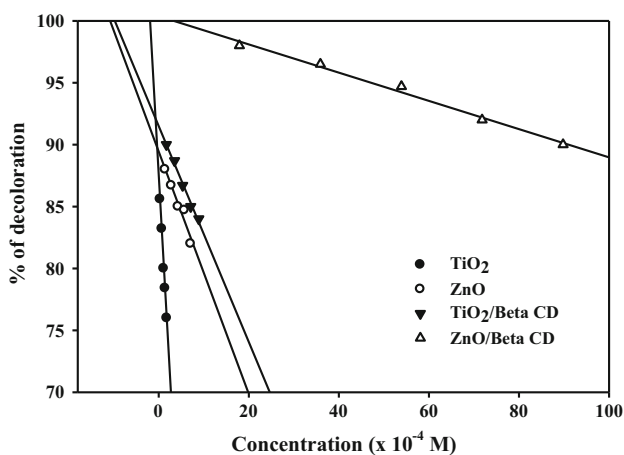
Fig. 8 *Effect of initial concentration* irradiation time = 120 min (TiO$_2$); 60 min (ZnO); 30 min (TiO$_2$/β-CD); 15 min (ZnO/β-CD); dose = 2 g/L (TiO$_2$ and ZnO); 0.2 g/L (TiO$_2$/β-CD and ZnO/β-CD), pH = 3.3
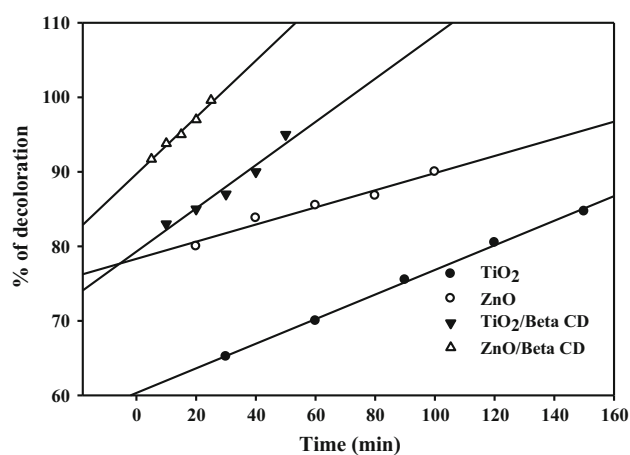
Fig. 9 *Effect of irradiation time* concentration = 1.1×10^{-4} M (TiO$_2$); 4.3×10^{-4} M (ZnO); 5.3×10^{-4} M (TiO$_2$/β-CD); 53.9×10^{-4} M (ZnO/β-CD), dose = 2 g/L (TiO$_2$ and ZnO), 0.2 g/L (TiO$_2$/β-CD and ZnO/β-CD), pH = 3.3

decoloration has been described by Langmuir–Hinshelwood. The Langmuir–Hinshelwood model can be written as follows

$$r = k \frac{K_{4-NP}[4-NP]}{1 + K_{4-NP}[4-NP]_0} = k_{obs}[4-NP] \tag{2}$$

$$\frac{1}{k_{obs}} = \frac{1}{kK_{4-NP}} + \frac{[4-NP]_0}{K} \tag{3}$$

where $[4-NP]_0$ is the initial concentration of 4-NP (M); K_{4-NP} the Langmuir–Hinshelwood adsorption equilibrium constant (M^{-1}) and k the rate constant of surface reaction (M/min):

$$\ln C_0/C_t = k_{obs}t \tag{4}$$

k_{obs} values for each initial concentration were found from the slopes of straight line obtained by plotting $\ln(C_0/C_t)$ versus reaction time t (Fig. 10a–d). When initial concentrations were plotted against $1/k_{obs}$, the rate constant and the adsorption equilibrium constant were calculated and found to be 0.189 mM/min (TiO_2), 0.224 mM/min (ZnO), 0.283 mM/min (TiO_2/β-CD) and 0.486 mM/min (ZnO/β-CD) and 59.28, 32.87, 15.03 and 10.72 mM respectively (Fig. 11) [24].
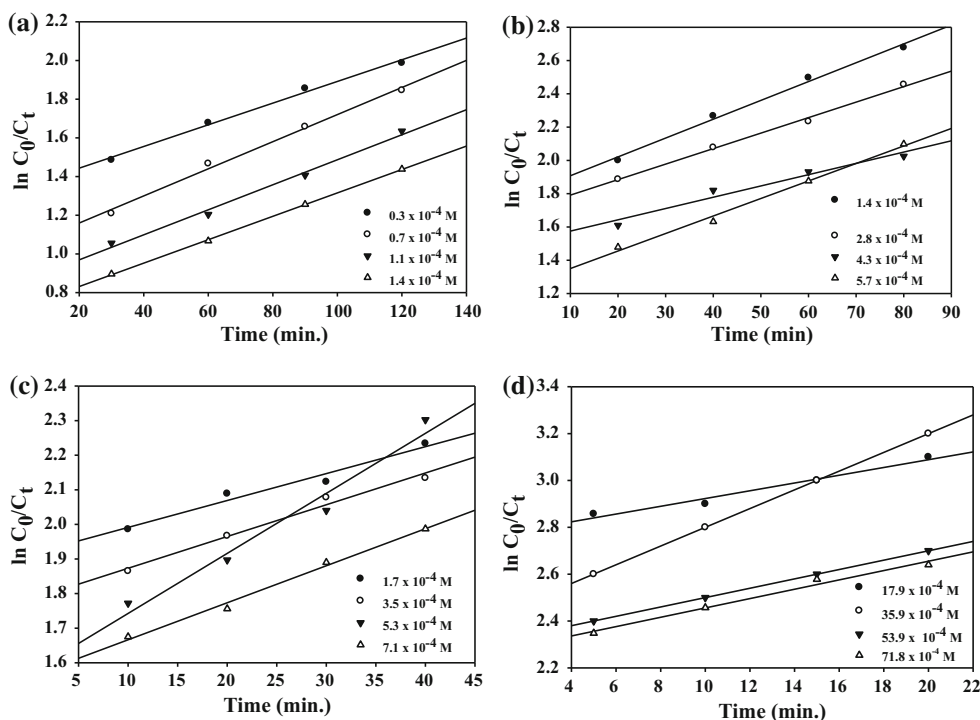
3.3.4 Effect of amount of catalysts

A series of experiments were carried out to assess the optimum amount of catalysts by varying the amount of catalyst from 1 to 5 g/L (TiO_2 and ZnO) and 0.1–0.5 g/L (TiO_2/β-CD and ZnO/β-CD). The results are presented in Fig. 12. It is interesting to note that the percentage of decoloration increases with increase in amount of catalysts from 78.0 to 92.6% for MO system and from 85.0 to 99.0% for MO/β-CD system. Enhancement of percentage of decoloration is due to (1) the increase in the amount of catalyst which increases the number of 4-NP molecules adsorbed and (2) the increase in the density of catalyst particles in the area of illumination. Our results are in accordance with the results of other researchers [25–27].

3.3.5 Effect of pH

The zero point charge for ZnO is 8.8 and TiO_2 is 6.2, and above this value the surface of the metal oxides is predominantly negatively charged when the pH is higher than the isoelectric point of metal oxides. Thus, the electrical property of the semiconductor metal oxide surface varies with the pH of the dispersion. Reactions were performed at different pH values under UV light irradiation. The role of pH in the photocatalytic decoloration was studied in the pH range of 2–10 at 2 g/L (TiO_2 and TiO_2/β-CD) and 0.2 g/L (ZnO and ZnO/β-CD) of catalysts. As shown in Fig. 13, the percentage of decoloration is found to be decreased with increase in pH from 88.0 to 74.0% for MO system and from 96.0 to 83.0% for MO/β-CD system. It is found that the percentage of photocatalytic decoloration at pH = 2 is

Fig. 10 Kinetics of photocatalytic decoloration a TiO_2, b ZnO, c TiO_2/β-CD, d ZnO/β-CD

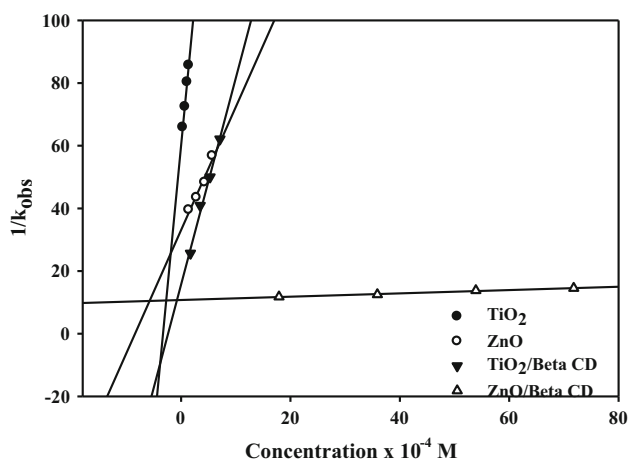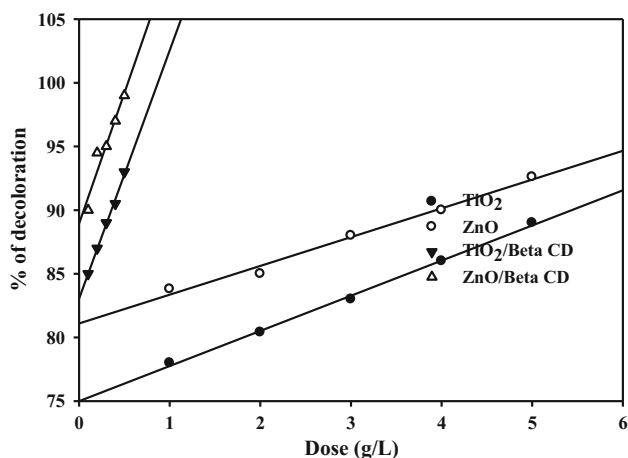**Fig. 11** Determination of the adsorption equilibrium constant and the reaction rate constant for 4-NP decoloration

Fig. 12 *Effect of amount of photocatalysts* concentration $= 1.1 \times 10^{-4}$ M (TiO$_2$); 4.3×10^{-4} M (ZnO); 5.3×10^{-4} M (TiO$_2$/β-CD); 53.9×10^{-4} M (ZnO/β-CD), irradiation time $= 120$ min (TiO$_2$); 60 min (ZnO); 30 min (TiO$_2$/β-CD); 15 min (ZnO/β-CD), pH $= 3.3$

higher than that at pH $= 10$. The results of our study resembling the reports of other researchers [21, 28, 29].

3.3.6 Determination of chemical oxygen demand (COD)

To confirm the mineralization of 4-NP, the decoloration was also analyzed by COD values. The COD value of 4-NP is increased with increase in pH (Fig. 14). This indicates the mineralization of 4-NP is high at acidic pH. Mineralization of 4-NP was also revealed by the formation of the smaller products viz. NH$_3$, CO$_2$ and H$_2$O during photocatalytic decoloration process. Our results are coinciding with the results of Zhang et al. [30] for the plasma-induced degradation of aqueous 2,4-dinitrophenol.
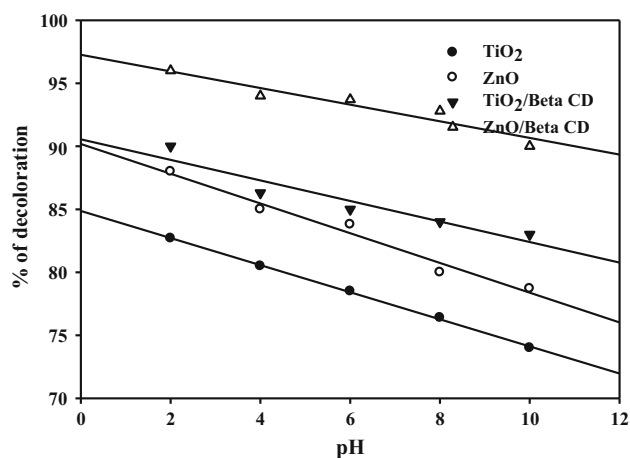

Fig. 13 *Effect of pH* concentration $= 1.1 \times 10^{-4}$ M (TiO$_2$); 4.3×10^{-4} M (ZnO); 5.3×10^{-4} M (TiO$_2$/β-CD); 53.9×10^{-4} M (ZnO/β-CD), irradiation time $= 120$ min (TiO$_2$); 60 min (ZnO); 30 min (TiO$_2$/β-CD); 15 min (ZnO/β-CD), dose $= 2$ g/L (TiO$_2$ and ZnO), 0.2 g/L (TiO$_2$/β-CD and ZnO/β-CD)

3.4 Mechanism for the enhancement of photocatalytic activity

A suitable mechanism for the photocatalytic decoloration of 4-NP with MO/β-CD is proposed as given below (Eqs i–ix) and also schematically represented in Fig. 15. 4-NP molecules enter into the cavity of β-CD, which is linked to the MO surface in the equilibrium stage. Since CDs have higher affinity on MO surface than 4-NP, β-CD molecules could adsorb on surface of the MO and occupy the reaction sites. β-CD would capture holes on active surface of MO resulting in the formation of stable MO/β-CD complex. Hence, the inclusion complex reaction of cyclodextrin with reactants such as MO/β-CD and 4-NP (Eq. ii) should be the key step in photocatalytic degradation in metal oxides suspension containing β-CD [31]. An electron is rapidly injected from the excited 4-NP to the conduction band. The
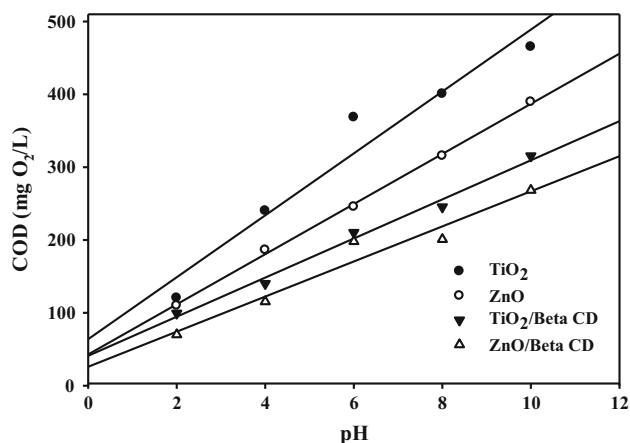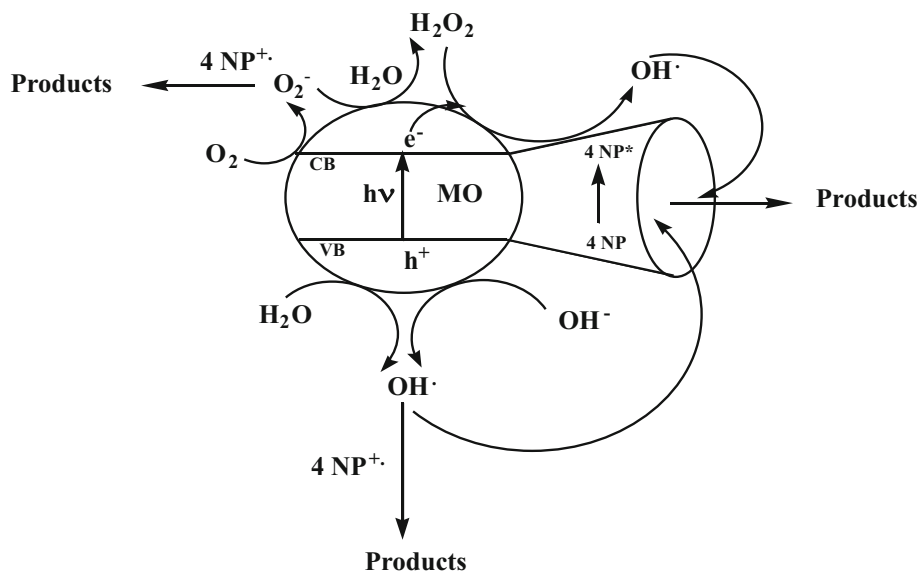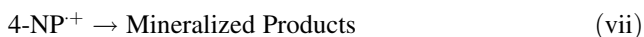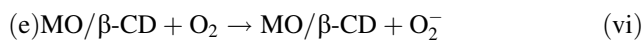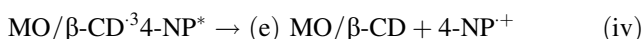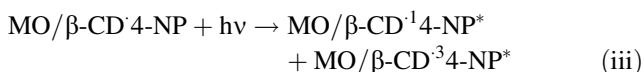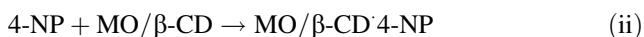

Fig. 14 Determination of COD

Fig. 15 Possible pathways for the photodecoloration of 4-NP on MO/β-CD

4-NP and 4-NP$^{+\cdot}$ radical then undergo decoloration (Eqs vii–ix) [32–35].

$$MO + \beta\text{-CD} \rightarrow MO/\beta\text{-CD} \tag{i}$$

$$4\text{-NP} + MO/\beta\text{-CD} \rightarrow MO/\beta\text{-CD}^{\cdot}4\text{-NP} \tag{ii}$$

$$MO/\beta\text{-CD}^{\cdot}4\text{-NP} + h\nu \rightarrow MO/\beta\text{-CD}^{\cdot 1}4\text{-NP}^* \\ + MO/\beta\text{-CD}^{\cdot 3}4\text{-NP}^* \tag{iii}$$

$$MO/\beta\text{-CD}^{\cdot 3}4\text{-NP}^* \rightarrow (e)\, MO/\beta\text{-CD} + 4\text{-NP}^{\cdot+} \tag{iv}$$

$$MO/\beta\text{-CD}^{\cdot 1}4\text{-NP}^* + O_2 \rightarrow MO/\beta\text{-CD}^{\cdot}4\text{-NP} + {}^1O_2 \tag{v}$$

$$(e)MO/\beta\text{-CD} + O_2 \rightarrow MO/\beta\text{-CD} + O_2^- \tag{vi}$$

$$4\text{-NP}^{\cdot+} \rightarrow \text{Mineralized Products} \tag{vii}$$

$$4\text{-NP} + {}^1O_2 \rightarrow \text{Mineralized Products} \tag{viii}$$

$$4\text{-NP} + {}^{\cdot}O_2^- \rightarrow \text{Mineralized Products} \tag{ix}$$

Based on the above results, it can be concluded that the enhancement of photocatalytic decoloration of 4-NP mainly results due to from enhanced adsorption of 4-NP on metal oxides surface and moderate inclusion depth of 4-NP in the β-CD cavity. Since β-CD can include into its cavity and is adsorbed onto the surface of metal oxides, it could play a role as "bridge" or "channel" for organic molecules to get onto the metal oxides surface and accumulate in higher concentrations, which makes 4-NP molecules decoloration more easily in the presence of hydroxyl radicals produced during photocatalytic decoloration processes. MO/β-CD exhibited apparently declined photoluminescence intensity compared with MO which indicated the electron/hole recombination has been suppressed in the MO/β-CD nanocomposite system. Therefore, the quantum efficiency of MO was enhanced since the

recombination of e_{CB}^-/h_{VB}^+ was decreased, which resulted in higher $^-$OH generation amount. Hence, the decoloration of 4-NP could be accelerated [36–40].

4 Conclusions

In all, a photocatalytic activity of MOs is enhanced by β-CD. On the basis of UV-DRS, FE-SEM and PXRD analyses the photocatalytic activity of MOs/β-CD can be attributed to two crucial factors: (1) the band gap energy of MOs/β-CD is lower than the corresponding metal oxides (2) phase structure and surface morphology of MOs remains unchanged in MOs/β-CD nanocomposites. Sequential photocatalytic decoloration of 4-NP under UV light revealed that MOs/β-CD possessed greater potential to be an effective and stable catalyst. MOs/β-CD could show significant photocatalytic activity mainly because β-CD could trap the photo generated holes resulting in the lower e_{CB}^-/h_{VB}^+ recombination. Furthermore, β-CD could play a role as ''channel'' or ''bridge'' between 4-NP and metal oxides, which facilitates the interaction between them.

References

1. C. Wang, B. Zhou, B. Huang, Water Sci. Eng. **8**, 20–29 (2015)
2. M.W. Chang, T.S. Chen, J.M. Chern, Ind. Eng. Chem. Res. **47**, 8533–8541 (2008)
3. E.L. Foletto, G.C. Collazzo, M.A. Mazutti, S.L. Jahn, Sep. Sci. Technol. **46**, 2510–2516 (2011)
4. I.M. El-Nahhal, S.M. Zourab, F.S. Kodeh, A.A. Elmanama, M. Selmane, I. Genois, F. Babonneau, J. Mater. Sci. Mater. Electron. **24**, 3970–3975 (2013)
5. B. Tian, C. Li, F. Gu, H. Jiang, Catal. Commun. **10**, 925–929 (2009)
6. D. Li, X. Wang, D. Wan, S. Duan, C. Liu, K. Zhang, B. Fang, Sep. Sci. Technol. **46**, 2539–2548 (2011)
7. A. Antony Muthu Prabhu, G. Venkatesh, N. Rajendiran, J. Fluoresc. **20**, 961–972 (2010)
8. E. Guivarch, S. Trevin, C. Lahitte, M.A. Oturan, Environ. Chem. Lett. **1**, 38–44 (2003)
9. S. Rajalakshmi, S. Pitchaimuthu, N. Kannan, P. Velusamy, Desalin. Water Treat. **52**, 3432–3444 (2014)
10. S. Pitchaimuthu, S. Rajalakshmi, N. Kannan, P. Velusamy, Desalin. Water Treat. **52**, 3392–3402 (2014)
11. S. Rajalakshmi, S. Pitchaimuthu, N. Kannan, P. Velusamy, Appl. Water Sci. (2014). doi:10.1007/s13201-014-0223-5
12. S. Pitchaimuthu, S. Rajalakshmi, N. Kannan, P. Velusamy, Appl. Water Sci. **5**, 201–208 (2015)
13. C. Karunakaran, G. Abiramasundar, P. Gomathisankar, G. Manikandan, V. Anandi, J. Colloid Interface Sci. **352**, 68–74 (2010)
14. Z. Zarghami, M. Maddahfar, M. Ramezani, J. Mater. Sci. Mater. Electron. **26**, 6339–6343 (2015)
15. C. Karunakaran, R. Dhanalakshmi, P. Gomathisankar, G. Manikandan, J. Hazard. Mater. **176**, 799–806 (2010)
16. C. Karunakaran, P. Gomathisankar, G. Manikandan, Mater. Chem. Phys. **123**, 585–590 (2010)
17. M. El-Kemary, H. El-Shamy, I. El-Mehasse, J. Lumin. **130**, 2327–2331 (2010)
18. K. Pitchumani, P. Velusamy, C. Srinivasan, Tetrahedron **50**, 12979–12988 (1994)
19. K. Pitchumani, P. Velusamy, H. Shayira Banu, C. Srinivasan, Tetrahedron Lett. **36**, 1149–1152 (1995)
20. P. Bansal, D. Sud, Sep. Purif. Technol. **85**, 112–119 (2012)
21. I.K. Konstantinou, T.A. Albanis, Appl. Catal. B **49**, 1–14 (2004)
22. D. Robert, B. Dongui, J.V. Weber, J. Photochem. Photobiol. A **156**, 195–200 (2003)
23. L. Pan, Z. Zhang, J. Mater. Sci. Mater. Electron. **21**, 1262–1269 (2010)
24. N. Daneshvar, D. Salari, A.R. Khataee, J. Photochem. Photobiol. A **157**, 111–116 (2003)
25. S. Irmak, E. Kusvuran, O. Erbatur, Appl. Catal. B **54**, 85–91 (2004)
26. S. Sakthivel, B. Neppolian, M.V. Shankar, B. Arabindoo, M. Palanichamy, V. Murugesan, Sol. Energy Mater. Sol. Cells **77**, 65–82 (2003)
27. J. Sun, L. Qiao, S. Sun, G. Wang, J. Hazard. Mater. **155**, 312–319 (2008)
28. T. Velegraki, D. Mantzavinos, Chem. Eng. J. **140**, 15–21 (2008)
29. H.H. Huang, D.H. Tseng, L.C. Juang, J. Hazard. Mater. **156**, 186–193 (2008)
30. J. Zhang, Z. Zheng, Y. Zhang, J. Feng, J. Li, J. Hazard. Mater. **154**, 506–512 (2008)
31. X. Zhang, F. Wu, Z. Wang, Y. Guo, N. Deng, J. Mol. Catal. A Chem. **301**, 134–139 (2009)
32. X. Zhang, F. Wu, N. Deng, J. Hazard. Mater. **185**, 117–123 (2011)
33. M.R. Hoffmann, S.T. Martin, W. Choi, D.W. Bahnemann, Chem. Rev. **95**, 69–96 (1995)
34. D.P. Macwan, P.N. Dave, S. Chaturvedi, J. Mater. Sci. **46**, 3669–3686 (2011)
35. G. Wang, F. Wu, X. Zhang, M. Luo, N. Deng, J. Hazard. Mater. B **133**, 85–91 (2006)
36. G. Wang, F. Wu, X. Zhang, M. Luo, N. Deng, J. Photochem. Photobiol. A **179**, 49–56 (2006)
37. P. Lu, F. Wu, N. Deng, Appl. Catal. B **53**, 87–93 (2004)
38. P. Velusamy, S. Rajalakshmi, S. Pitchaimuthu, N. Kannan, Indian J. Environ. Protect. **31**, 801–809 (2011)
39. P. Velusamy, S. Pitchaimuthu, S. Rajalakshmi, N. Kannan, J. Adv. Res. **5**, 19–25 (2014)
40. X. Zhang, F. Wu, N. Deng, Catal. Commun. **11**, 422–425 (2010)